

$^4\text{He}/\text{H}_2$ binary clusters: A path-integral Monte Carlo study

M. C. Gordillo

Departament de Física i Enginyeria Nuclear, Campus Nord B4-B5, Universitat Politècnica de Catalunya, E-08034 Barcelona, Spain

(Received 26 February 1999)

The structure and thermodynamic properties of the $^4\text{He}/\text{H}_2$ binary clusters are studied by path-integral Monte Carlo simulations. It has been found that, despite their lower mass, the H_2 molecules form a subcluster of their own at the center of the system. When the number of helium atoms increases for a fixed number of hydrogen molecules, those inner clusters get compressed but retain their original form. The fraction of H_2 in the superfluid state decreases with the subcluster compression, but remains finite for small H_2 concentrations. [S0163-1829(99)01433-2]

INTRODUCTION

The study of clusters has been a prolific field both from the experimental and theoretical point of view.¹⁻³ The change in these systems as the number of particles increases provides a unique look at how the bulk properties emerge and allows us to study characteristics with no counterpart in the thermodynamic limit. In particular, the behavior of doped and binary clusters has attracted much attention. For instance, simulation studies of classical binary Lennard-Jones clusters^{4,5} show a rich phase diagram depending on the relative depth of the potential wells and on the size of the particles involved. For a concentration ratio 1:1 the center of the cluster tends to be occupied by the species with the larger ϵ_{LJ} and the lower σ_{LJ} . When the difference in the Lennard-Jones parameters decreases, the separation is less apparent and disappears for species *A* and *B* when $\epsilon_{AA} \sim \epsilon_{AB} \sim \epsilon_{BB}$ and $\sigma_{AA} \sim \sigma_{AB} \sim \sigma_{BB}$.

The consideration of the quantum nature of the species introduces additional effects. In this case, the degree of delocalization of particles of type *A* and *B* differs, being greater for particles with lower mass. The consequences of the differences in the zero-point energies in quantum clusters have been studied in the case of isotopic mixtures of helium ($^3\text{He}/^4\text{He}$),⁶⁻⁸ hydrogen (H_2/D_2),^{9,10} and neon ($^{20}\text{Ne}/^{22}\text{Ne}$).¹¹ In all these calculations, in which the interparticle potential does not distinguish the isotopic character of the components, the heaviest particle is more probably found in the inner regions of the cluster. Naturally, this effect is larger when the differences in the isotope masses increase.

There are also theoretical studies covering what happens when quantum effects are taken into account together with different interaction parameters (ϵ and σ in the Lennard-Jones case). However, they consider only the situation of a single impurity in a quantum cluster. The type of impurities ranges from an alkali metal atom (Li) in H_2 clusters¹² to big molecules as Cl_2 and SF_6 in ^4He clusters.^{13,14} In this last case, one has also the opportunity of comparing the results with experimental data.¹⁵⁻¹⁷ Since these impurities are heavier than a hydrogen molecule or a helium atom, it was observed that their location in the cluster depended on the impurity-medium interaction. If that potential well is smaller than that corresponding to the pure fluid, the impurity stays

at the surface of the system (Li), otherwise, it is located close the center. When the latter happens, the impurity can be used as a probe to test if the liquid around is a superfluid. For instance, the differences in the vibrational spectrum of OCS in and out of a helium cluster has recently served to probe the superfluidity of the ^4He atoms in a small cluster.¹⁸

What all these systems have in common is that they consider the case of a classical or nearly classical impurity (big mass) in a quantum environment (He or H_2). Apparently, there is only one study of what happens when both components are different and both of quantum nature. Whaley and co-workers^{13,19,20} carried out VMC and DMC simulations of ^4He clusters with a single H_2 impurity. In that case, all the effects described above compete: on one hand, the H_2 -He interaction is deeper the He-He one, which favors the impurity in the center of the cluster and, on the other, the mass of the hydrogen molecule is approximately half of the mass of a ^4He atom. The latter would make the impurity migrate to the surface of the system. The results indicate that the mass effects predominate: the H_2 is delocalized, going from the inside to the outside of the cluster almost freely. However, no account has been given of what happens when several H_2 molecules are included in a ^4He cluster, and how this affects the cluster properties. That is part of the objectives of the present work. At the same time, it is also interesting to check how the presence of one component influences the superfluidity of the other in binary clusters. It has been predicted that small clusters of both pure ^4He and *p*- H_2 become superfluids if the temperature is low enough.^{21,22} On the other hand, it is known that big impurities tend to reduce the superfluidity in helium clusters,¹⁹ so the comparison of this case with the one with several small impurities could be informative. That aspect will be also analyzed.

METHOD

The path-integral Monte Carlo (PIMC) method is a numerical tool that allows us to calculate the thermodynamic and structural properties of a quantum system at finite temperature. The technique is essentially exact, the only necessary input being the potential between the different pairs of species. With that, the basic ingredient of the method, the density matrix for a given temperature *T*, can be written

$$\rho(R, R'; \beta) = \langle R | \exp(-\beta H) | R' \rangle, \quad (1)$$

where $\beta=1/k_B T$ (k_B is the Boltzman constant), H is the Hamiltonian of the system, and R represents a set of $3N$ coordinates corresponding to the N particles considered. The expected value of any operator O is given by the expression:

$$\langle O \rangle = \frac{1}{Z} \int dR dR' \langle R | O | R' \rangle \rho(R, R'; \beta), \quad (2)$$

where

$$Z = \int dR \rho(R, R'; \beta) \quad (3)$$

is the partition function.

Unfortunately, this approach is not directly applicable since one does not know the density matrix at the low temperatures of interest. However, one can obviate that by expanding the matrix in the form,

$$\rho(R, R'; \beta) = \int \cdots \int dR_1 dR_2 \cdots dR_{M-1} \rho(R, R_1; \tau) \times \rho(R_1, R_2; \tau) \cdots \rho(R_{M-1}, R'; \tau), \quad (4)$$

where $\tau = \beta/M$. Here, $M-1$ complete sets of $3N$ coordinates are introduced. That can be visualized as if each particle were described by a chain of $M+1$ *time slices* or *beads* (M in the diagonal form) instead of the customary $3N$ coordinates of the classical simulations. That allows the calculation of the properties of the system at temperature T by using the density matrices corresponding to temperatures M times bigger. The higher the temperature, the closer the density matrix would be to a classical one, and the easier it will be to obtain.²³

Since both ${}^4\text{He}$ and $p\text{-H}_2$ are bosons, one has to take also into account the symmetrization of the density matrices. Thus,

$$\rho_B(R, R'; \beta) = \frac{1}{N_{\text{He}}!} \frac{1}{N_{\text{H}_2}!} \sum \rho(R, P R'; \beta), \quad (5)$$

where P indicates all the possible particle index permutations between identical particles. After that, only the expressions for the interatomic potentials are needed. For the helium-helium interaction, the updated potential of Aziz *et al.*²⁴ was employed. This potential is slightly more attractive than previous ones. For the hydrogen-hydrogen potential the Silvera and Goldman's parametrization was used.²⁵ The latter gives a spherical average form for the $\text{H}_2\text{-H}_2$ interaction, that was found to reproduce experimental data in a study about melting of hydrogen surfaces.^{26,27} The $V_{\text{H}_2\text{-He}}$ potential has been taken from Ref. 19, in which the properties of a single H_2 impurity in a ${}^4\text{He}$ cluster were theoretically analyzed. Since all clusters are metastable with respect to evaporation, they were surrounded by a confining wall to avoid the flying out of particles. Following Ref. 11, a potential of the form

$$V = \epsilon \sum_i \left(\frac{R_i - R_{\text{cm}}}{R_c} \right)^{20} \quad (6)$$

was used, ϵ is the well depth of the Lennard-Jones part of the $\text{H}_2\text{-He}$ potential mentioned above¹⁹ (13.6 K). R_{cm} is the position of the center of mass of the whole cluster, that is always kept in the center of the simulation cell. To be sure of that, its position after each accepted movement in the Monte Carlo procedure was corrected. R_c is a parameter that indi-

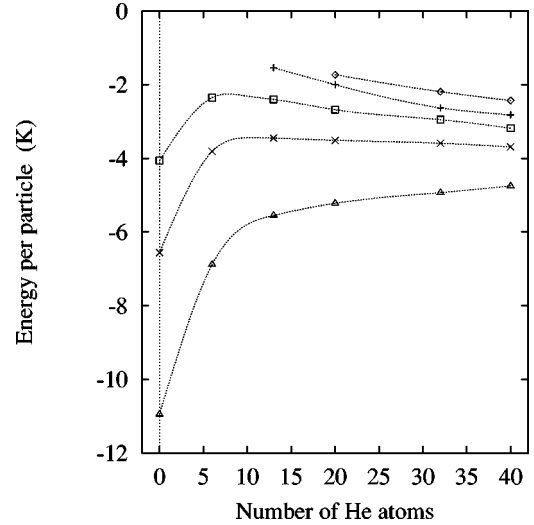


FIG. 1. Energy per particle (K) versus number of ${}^4\text{He}$ atoms for different hydrogen compositions. From top to bottom, we have $N_{\text{H}_2}=0$ (diamonds), $N_{\text{H}_2}=2$ (plus), $N_{\text{H}_2}=3$ (squares), $N_{\text{H}_2}=4$ (crosses), $N_{\text{H}_2}=6$ (triangles). Error bars are smaller than the size of the symbols.

cates where the confining potential starts to be important. In all simulations, $R_c = 6\sigma$, σ being the $\text{H}_2\text{-He}$ Lennard-Jones parameter in Ref. 19 ($\sigma = 3 \text{ \AA}$). Nevertheless, it has been checked that the final results do not vary when these parameters are slightly changed.

One of the potential problems of studying binary clusters is the possible existence of metastable states. In particular, one can have the wrong species in the center of the cluster. To avoid that, an algorithm that allowed the interchange of particles was designed. After having tried to move each particle of the cluster, the position of each H_2 molecule was switched with a randomly chosen ${}^4\text{He}$ atom. If the change in the action was favorable, the new configuration was taken, otherwise, the old one was kept. In the equilibration period, the percentage of interchanges is quite high ($>20\%$) but after that is greatly reduced ($\sim 1\%$). Similar results are obtained when different initial configurations were used.

The temperature was set to 0.5 K in all simulations. This temperature is low enough to allow many cluster combinations to be stable and high enough not to make the computations very demanding. The pair action approximation²³ was used. That means that the total action for the system was constructed from the exactly solved action for a pair of particles, which reduces greatly the number of *time slices* needed in the calculations. Thus, τ was chosen to be $1/80 \text{ K}$, what implies that for $\beta = 2 \text{ K}^{-1}$, $M = 160$ *time slices* were used. This τ has been shown to be accurate for pure H_2 clusters.²⁸ Several small clusters with the number of hydrogen molecules between 2 and 13, and helium atoms ranging from 0 to 40 for each H_2 composition, have been studied.

RESULTS

Figure 1 displays the energy per particle versus the number of helium atoms in the system for all the clusters that do not evaporate after 10^5 Monte Carlo steps. The symbols correspond to simulation results and the lines are guides to the

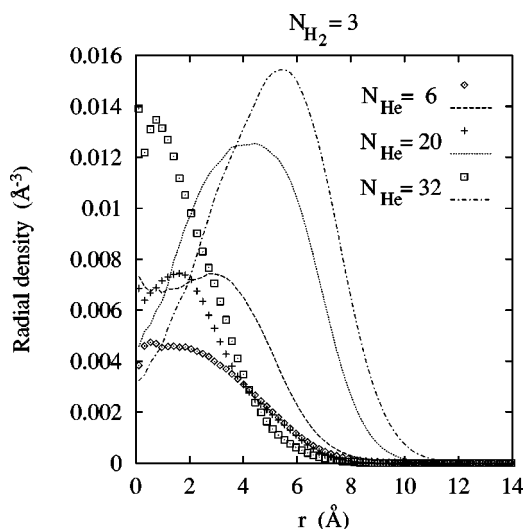


FIG. 2. Density profiles for hydrogen (symbols) and helium (lines) when N_{H_2} is kept fixed and equal to 3. See text for details.

eye. As it was mentioned above, the temperature was set to 0.5 K in all cases. In those simulation conditions, the calculations indicate that clusters with less than two hydrogen molecules *and* less than 20 helium atoms evaporate completely, irrespectively of the initial particle configuration. It was observed that, to avoid decomposition, an energy per particle lower than ~ -1.5 K is needed. However, Whaley and co-workers,^{13,19,20} employing zero-temperature algorithms (no thermal excitations) found that small clusters are bound even when the total number of particles was three.^{13,19,20} Nevertheless, for bigger pure clusters of helium atoms, the energies found here are compatible with their zero-temperature results, even taking into account that the Aziz potential used here is slightly more attractive than the one used in Ref. 19 ($E/N = -1.688 \pm 0.002$ in Ref. 20 for He_{20} and -1.73 ± 0.04 in the present work).

When $N_{H_2} < 4$, and $N_{He} > 10$, the energy per particle of the whole cluster decreases with the number of 4He atoms present. This implies that N_{H_2} is not large enough to disturb appreciably the energy trend of a pure helium cluster. On the other hand, the hydrogen influence is appreciable when $N_{He} < 10$. There, the energy per particle increases with the number of helium atoms due to the difference between the He-He and H_2 - H_2 potential wells. In any case, the asymptotic energy limit for big helium clusters [the bulk energy per particle -7.17 K (Ref. 29)] is far from being reached in the clusters considered here.

There is also a change in the density profiles with respect to the results of Ref. 19. When $T=0$ and only one H_2 molecule is present, the maximum in the hydrogen density profile is located out of the center of the system. This is not so when $N_{H_2} > 1$. The effect is depicted in Figs. 2 and 3. Figure 2 displays the density distributions of clusters with three hydrogen molecules and a variable number of helium atoms. The origin of those curves is the center of mass of the whole system. The symbols indicate the hydrogen concentration and the lines indicate the concentration of the helium. One can see that the probability of finding a H_2 molecule increases when we go from the outside to the inner regions of the cluster. This trend can be safely identified despite the

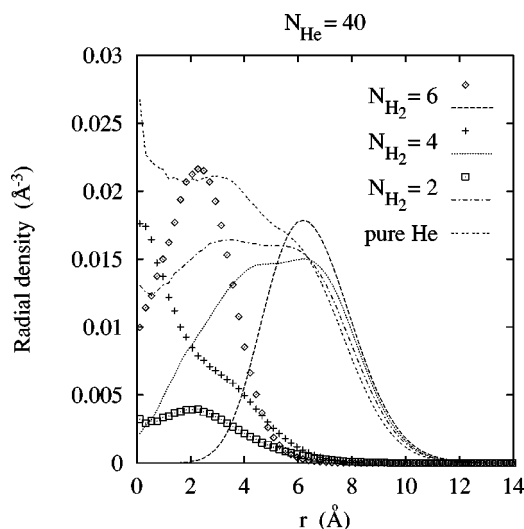


FIG. 3. Same than in Fig. 2 but keeping constant the helium distribution and varying the hydrogen one.

relatively large statistical errors at small r 's. The maximum in the helium distribution also increases (simply because there are more atoms) and what is more relevant, shifts towards bigger distances of the center of mass. This effect is accompanied by a depletion of the helium density in the innermost zones of the cluster. As in a pure cluster, no shells are observed in the helium coating. That indicates that the ‘‘impurity’’-helium interaction is not strong enough to create layers, as in the case of big molecules such as SF_6 .¹⁴

The variation of the density profiles when N_{He} is constant and N_{H_2} is not is shown in Fig. 3. For $N_{H_2}=2$, the situation is again different than of the $N_{H_2}=1$ case in Ref. 19: the hydrogen molecules are completely surrounded by helium. This is also the case when one considers more H_2 in the cluster. Obviously, when the number of hydrogen molecules increases, there is a correlated depletion of the helium presence in the center of the cluster. One can see also that about six hydrogen molecules are needed to decrease the He density to zero when $r \rightarrow 0$. Incidentally, the density profile for the pure helium case is virtually identical to those displayed in Ref. 7 for a cluster with the same number of helium atoms, and very similar to the one shown in Ref. 22 for $N_{He}=64$. As in the cases displayed in Fig. 2, there are no signs of layering in the helium coating.

All the density profiles suggest that the hydrogen molecules are close to one another. This is also sound from the energetic point of view: the H_2 - H_2 interaction is much larger than the He-He or the He- H_2 ones. To test further if there are H_2 subclusters the radial distribution functions [$g(r)$'s] for the hydrogen-hydrogen pairs were calculated. Figure 4 displays the results for $N_{H_2}=4$ for six different helium coatings. One observes that the form of the cluster is quite maintained in the whole 4He concentration interval. The only appreciable differences are an increase of the density of the main peak and a correlated decrease of the density at the tail of the distribution. One can see also that the hydrogen subcluster is a compact structure, with only one peak corresponding to a nearest-neighbor distance of ~ 3.8 Å, similar than in bulk. The position of that peak does not change when the whole cluster becomes bigger and the form of the entire $g(r)$ re-

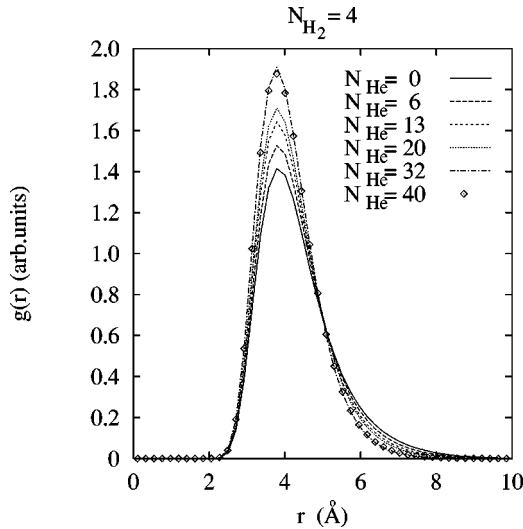


FIG. 4. H_2 - H_2 radial distribution functions in arbitrary units for $N_{\text{H}_2}=4$ and different helium concentrations.

mains constant for $N_{\text{He}} > 32$. This is probably the compression limit for this cluster, and it would not vary even if it is surrounded with bulk helium. Something similar happens when $N_{\text{H}_2}=13$, for the same range of ${}^4\text{He}$ concentrations (Fig. 5). Now a $g(r)$ with two H_2 layers emerges, corresponding to the more or less icosahedral structure found in Ref. 21. As in the case of $N_{\text{H}_2}=4$, one has a compact structure whose form remains constant when the number of helium atoms increases. The compression is even smaller that in the previous case: the radial distribution function does not change appreciably for $N_{\text{He}} > 20$.

It has been predicted that H_2 clusters with $N_{\text{H}_2} < 20$ would be superfluid if the temperature is low enough.²¹ One can ask how that superfluidity would be affected by the presence of ${}^4\text{He}$ atoms. To check that, the fraction of H_2 molecules in the superfluid has been calculated for different helium concentrations. That was made for the two hydrogen subclusters

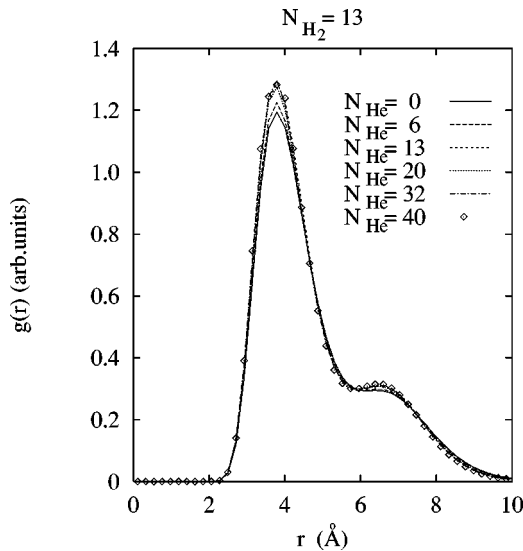


FIG. 5. Same than in Fig. 4 for $N_{\text{H}_2}=13$. The y scale is also the same than in Fig. 4.

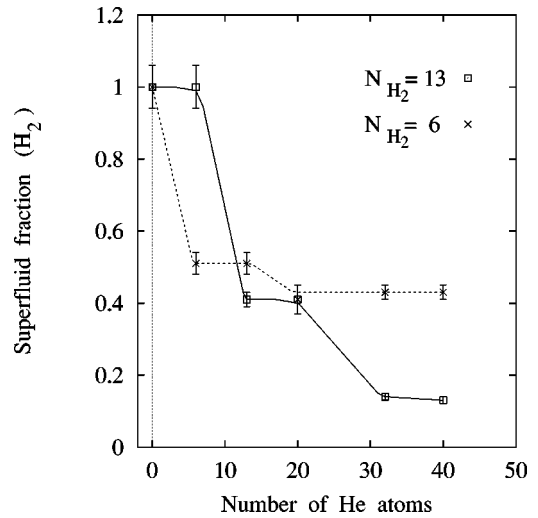


FIG. 6. Superfluid fraction in the hydrogen subclusters as a function of the number of helium atoms.

that should be superfluids according to Ref. 21 ($N_{\text{H}_2}=6,13$). The superfluid fraction (ρ_s/ρ) is calculated by²³

$$\frac{\rho_s}{\rho} = \frac{4m^2 \langle A_z \rangle}{\beta \hbar^2 I_c}, \quad (7)$$

where $\langle A_z \rangle$ is the area swept out by the paths in the xy plane and I_c is the classical moment of inertia of the H_2 subcluster.²³ The results are reported in Fig. 6 for $N_{\text{H}_2}=6,13$. When no helium atoms are present, the results coincide with those of Ref. 21: all the molecules in the cluster are part of the superfluid. However, in the $N_{\text{H}_2}=6$ cluster this situation changes immediately when some helium is added, with the superfluid fraction decreasing up to ~ 0.5 . This value is kept for $N_{\text{He}}=13$, but it dwindles again to ~ 0.41 when $N_{\text{He}} > 20$. No further variation is seen even for the biggest cluster considered. When $N_{\text{H}_2}=13$ the situation is basically the same, the only difference being the helium concentrations at which the ‘‘jumps’’ in the superfluid values are

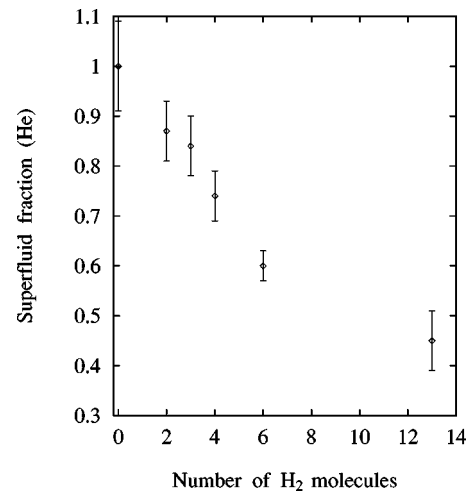


FIG. 7. Same than in Fig. 6 but in the helium coating ($N_{\text{He}}=40$).

registered ($N_{\text{He}}=13$ instead of $N_{\text{He}}=6$ and $N_{\text{He}}=32$ instead of $N_{\text{He}}=20$). The fact that the superfluid fraction tends to be constant for high N_{He} suggests that once the subcluster is completely surrounded by ^4He , this value remains essentially the same. Since the structures of the inner clusters do not change for $N_{\text{He}}>32$ (see Figs. 4 and 5), it is reasonable to suppose that the limit for $N_{\text{He}}=40$ is (or very close to) the superfluid H_2 fraction for clusters in bulk helium. On the other hand, when N_{He} is small, one needs to have an appreciable helium concentration to make $\rho_s/\rho \neq 1$ ($N_{\text{He}}/N_{\text{H}_2}=1$ for both hydrogen subclusters).

Figure 7 shows the variation of the superfluid fraction for a fixed He composition ($N_{\text{He}}=40$) when the number of H_2 molecules increases. As in the hydrogen case, when no other particles are present, all atoms are in the superfluid state, but ρ_s/ρ decreases when the hydrogen concentration increases. This behavior is similar to the one reported in Ref. 14 for a system of 39 ^4He atoms with a single SF_6 impurity. In that work, for $T=0.625$ K the superfluid fraction was 0.67. In Fig. 7 it can be observed that this would correspond to approximately six hydrogen molecules. Thus, in both cases, the presence of impurities depletes the superfluid state, and in the present case, this depletion is larger when N_{H_2} increases.

CONCLUSIONS

The structure and thermodynamic properties of $^4\text{He}/\text{H}_2$ binary clusters have been studied using the PIMC method. It was found that, contrary to what happened when only one H_2 is present, the hydrogen tends to be located in the inner regions of the cluster. That means that the energetic effects ($\epsilon_{\text{H}_2-\text{H}_2} > \epsilon_{\text{He}-\text{He}}$) are more important than the quantum delocalization ($m_{\text{H}_2} \sim 1/2m_{\text{He}}$). The H_2 forms subclusters of their own in the center of the system, with basically the same structure as their isolated counterparts. The only difference is the behavior of the superfluid density: for the same number of H_2 molecules, the superfluid fraction decreases with the number of He atoms in the cluster. Something similar happens when the number of helium atoms is kept fixed and the hydrogen concentration varies.

ACKNOWLEDGMENTS

This work was carried out using the computer facilities at NCSA. I thank the Spanish Ministry of Education and Culture (MEC) for a postgraduate contract. I also thank very specially J. Boronat for a careful reading of the manuscript and D. Ceperley, J. Boronat, and L. Brualla for thoughtful discussions.

-
- ¹R. S. Berry, T. L. Beck, H. I. Davis, and J. Jellinek, *Adv. Chem. Phys.* **70**, 17 (1988).
- ²K. B. Whaley, *Int. Rev. Phys. Chem.* **13**, 41 (1994).
- ³W. Schoelkopf and J. P. Toennies, *Science* **266**, 1345 (1994).
- ⁴A. S. Clarke, R. Kapral, B. Moore, G. Patey, and X. G. Wu, *Phys. Rev. Lett.* **70**, 3283 (1993).
- ⁵A. S. Clarke, R. Kapral, and G. N. Patey, *J. Chem. Phys.* **101**, 2432 (1994).
- ⁶A. Belic, F. Dalfovo, S. Fantoni, and S. Stringari, *Phys. Rev. B* **49**, 15 253 (1994).
- ⁷S. A. Chin and E. Krotscheck, *Phys. Rev. B* **52**, 10 405 (1995).
- ⁸M. Barranco, M. Pi, S. M. Gatica, E. S. Hernandez, and J. Navarro, *Phys. Rev. B* **56**, 8997 (1997).
- ⁹C. Chakravarty, *Phys. Rev. Lett.* **75**, 1727 (1995).
- ¹⁰C. Chakravarty, *J. Chem. Phys.* **104**, 7223 (1996).
- ¹¹C. Chakravarty, *J. Chem. Phys.* **102**, 956 (1995).
- ¹²D. Scharf, G. J. Martyna, and M. L. Klein, *J. Chem. Phys.* **99**, 8997 (1993).
- ¹³R. N. Barnett and K. B. Whaley, *Z. Phys. D* **31**, 75 (1994).
- ¹⁴Y. Kwon, D. M. Ceperley, and K. B. Whaley, *J. Chem. Phys.* **104**, 2341 (1995).
- ¹⁵S. Goyal, D. L. Schutt, and G. Scoles, *Phys. Rev. Lett.* **69**, 933 (1992).
- ¹⁶R. Frochtenicht, J. P. Toennies, and A. Vilesov, *Chem. Phys. Lett.* **229**, 1 (1994).
- ¹⁷M. Hartmann, R. B. Miller, J. P. Toennies, and A. Vilesov, *Phys. Rev. Lett.* **75**, 1566 (1995).
- ¹⁸S. Grebenev, J. P. Toennies, and A. F. Vilesov, *Science* **279**, 2083 (1998).
- ¹⁹R. N. Barnett and K. B. Whaley, *J. Chem. Phys.* **96**, 2953 (1992).
- ²⁰R. N. Barnett and K. B. Whaley, *Phys. Rev. A* **47**, 4082 (1993).
- ²¹P. Sindzingre, D. M. Ceperley, and M. L. Klein, *Phys. Rev. Lett.* **67**, 1871 (1991).
- ²²P. Sindzingre, M. L. Klein, and D. M. Ceperley, *Phys. Rev. Lett.* **63**, 1601 (1989).
- ²³D. M. Ceperley, *Rev. Mod. Phys.* **67**, 279 (1995).
- ²⁴R. A. Aziz, A. R. Janzen, and M. R. Molvoder, *Phys. Rev. Lett.* **74**, 1586 (1995).
- ²⁵I. F. Silvera and V. V. Goldman, *J. Chem. Phys.* **69**, 4209 (1978).
- ²⁶M. Wagner and D. M. Ceperley, *J. Low Temp. Phys.* **89**, 581 (1992).
- ²⁷M. Wagner and D. M. Ceperley, *J. Low Temp. Phys.* **102**, 275 (1996).
- ²⁸C. Chakravarty, M. C. Gordillo, and D. M. Ceperley, *J. Chem. Phys.* **109**, 2123 (1998).
- ²⁹R. De Bruyn Ouboter and C. N. Yang, *Physica B* **39**, 2700 (1987).